CERN/PS 85-67 (LI)
September 15, 1985

COMPUTER PROGRAMS AND METHODS FOR THE DESIGN OF HIGH INTENSITY RFQs

C. Biscari*

---

*from the University of Naples, Italy

INTRODUCTION

The idea of bunching, focusing and accelerating a continous beam of ions by a radio frequency quadrupole was proposed in the late sixties by Kapchinskii [1] who called the device a "spatially continous quadrupole focusing" machine. The first realization in the occidental world of such a device was done in Los Alamos National Laboratory in 1980 [2]

At CERN an RFQ accelerator (RFQ1) is working remarkably well as a preinjector of the LINAC1 for protons since march 1984 [4] having been before in test operation for nearly one year. The substitution by another RFQ (RFQ2) of the Cockcroft Walton and low energy beam transport of the LINAC2 is foreseen in near future.

This report has been conceived in order to collect information concerning the design of an RFQ from the point of view of beam optics, and although most of the topics have been treated elsewhere they have been included here for the sake of completeness. The whole material has been worked out in collaboration with M. Weiss, during the design study of the RFQ2.

A first chapter is dedicated to the detailed derivation of the electric field to which particles are submitted inside the accelerator. The description of different sections of the RFQ follows, and here we have benefited from the Los Alamos methods. Another chapter treats the current limits and the space charge forces. The computer programs used at CERN for the design of an RFQ are described subsequently, and finally the electric surface fields and the vane machining are treated.

1. ELECTRIC POTENTIAL AND FIELD

1.1 Electric potential

The bunching, acceleration and focusing of the beam inside the RFQ is performed by the electric field generated by four electrodes (vanes) arranged in a quadrupolar symmetry around the longitudinal axis, and excited by rf power.

The electrodes of the RFQ are designed according to specific requirements, the only fact being fixed that they must combine the quadrupolar azimuthal symmetry which focuses the beam transversally with a longitudinal modulation which accelerates and/or bunches the particles.

The alternating focusing is obtained from the alternating electric gradient and, unlike the magnetic focusing force, is constant for any velocity of the particles. The longitudinal component of the electric field responsible for the acceleration, bunching, etc. is determined by the shape of the unit cells of length $\beta\lambda/2$, which compose the structure (see Figure1). β is the velocity of the synchronous particle in units of the velocity of light c, and λ is the wavelength of the rf.

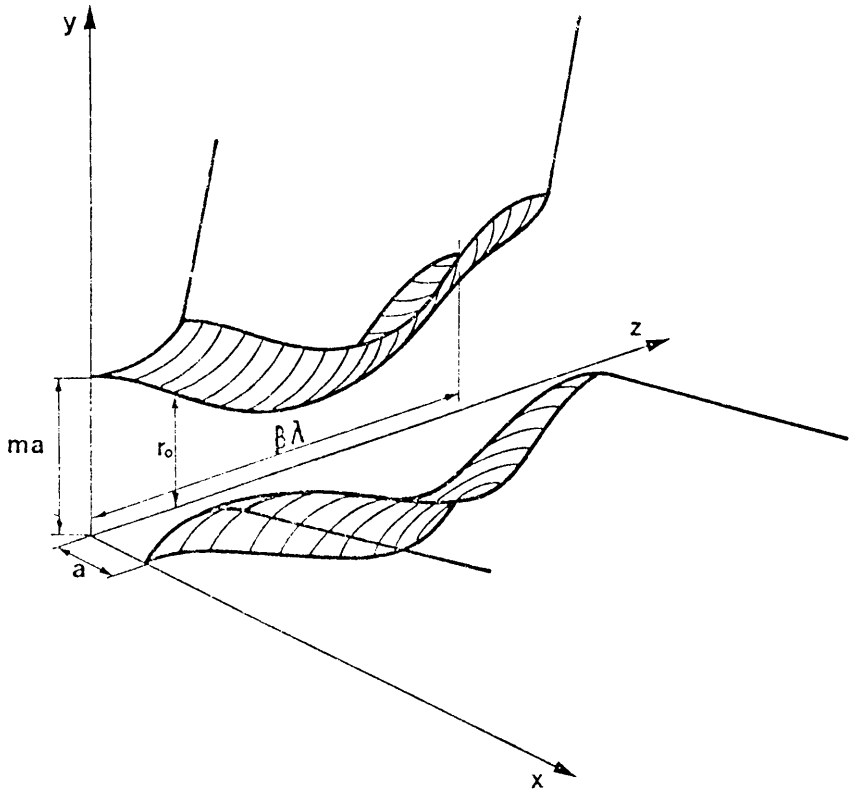

Figure 1: Shape of two adjacent vanes for a $\beta\lambda$ period

The wave equation in the region near the axis can be approximated by the Laplace equation

$$\nabla^2 U = 0 \tag{1.1.1}$$

being U the electric field potential, from which the forces acting on the particles can be derived. The solution of eq.(1.1.1) can be written in cylindrical coordinates as the product of three functions, each of them depending only on one of the variables, r, θ or z:

$$U(r,\theta,z) = R(r)\,\Theta(\theta)\,Z(z) \tag{1.1.2}$$

This equation represents the spatial configuration of the electric potential. Its complete specification is obtained multiplying it by the time variation of the rf: $\sin(\omega t+\psi)$, being $\omega = 2\pi c/\lambda$.

The functions R(r), $\Theta(\theta)$, and Z(z) have to satisfy the symmetries of the structure.

1.2 Quadrupolar symmetry

The first condition is the quadrupolar symmetry, which is expressed in the polar coordinates r and θ. The Laplace equation in polar coordinates is:

$$\Theta(\theta)\partial^2 R(r)/\partial r^2 + (1/r)\Theta(\theta)\partial R(r)/\partial r + (1/r^2)R(r)\partial^2\Theta(\theta)/\partial r^2 = 0 \tag{1.2.1}$$

Let's study first the dependence on the angular variable. $\Theta(\theta)$ can be expressed generally as a series in sine and cosine,

$$\Theta(\theta) = \Sigma_n a_n \cos n\theta + \Sigma_p b_p \sin p\theta \tag{1.2.2}$$

and has to satisfy three conditions (see Figure 2):

i) $\Theta(\theta) = \Theta(-\theta)$

This equation is equivalent to : $b_p \sin p\theta = -b_p \sin p\theta$, which implies that $b_p = 0\ \forall p$.

ii) $\Theta(\theta) = \Theta(\pi-\theta)$

which means : $\cos n\theta = \cos n(\pi-\theta) \rightarrow \cos n\theta = 1$ and n must be even

iii) $\Theta(\theta) = -\Theta(\pi/2 - \theta)$

that is, $\cos 2l\theta = -\cos l\pi \cos 2l\theta \rightarrow \cos l\pi = -1$, so l must be odd.

The function $\Theta(\theta)$ can then be written as

$$\Theta(\theta) = \Sigma_n a_n \cos 2(2n+1)\theta \tag{1.2.3}$$

Substituting $\Theta(\theta)$ in Eq.(1.2.1) we obtain the differential equation for R(r):

$$\Sigma_n[r^2\partial^2 R(r)/\partial r^2 + r\partial R(r)/\partial r - 4(2n+1)^2 R(r)] = 0 \tag{1.2.4}$$

The summation goes from $n=0$ to $n=\infty$.

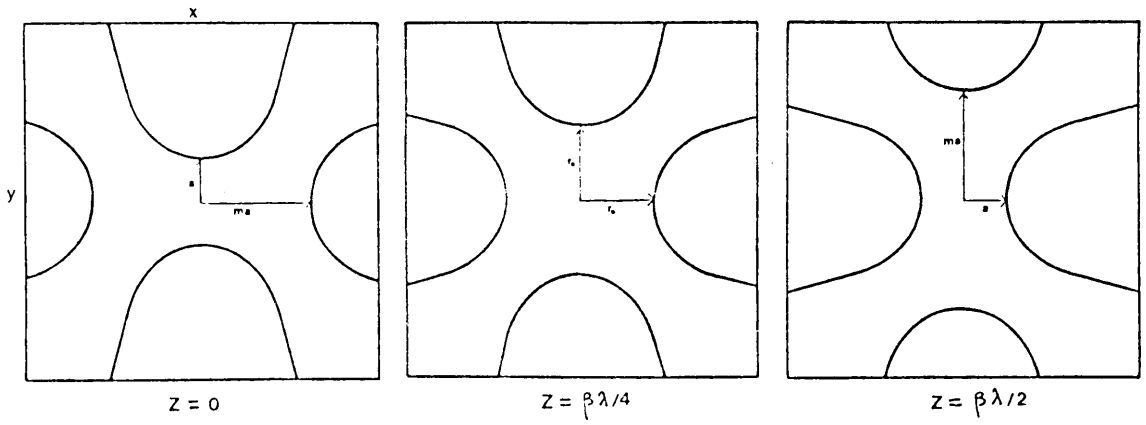

Figure 2: Transverse sections of the cell

The corresponding solution is:

$$R(r) = \Sigma_n a_{rm} r^{2(2n+1)} \tag{1.2.5}$$

The potential which represent the quadrupolar symmetry is then

$$U(r,\theta) = \Sigma_n c_n r^{2(2n+1)} \cos 2(2n+1)\theta \tag{1.2.6}$$

1.3 Longitudinal modulation

We add now the variation along z.

Let's express the potential function as $U_1(r,\theta,z) = R_1(r)\Theta_1(\theta)Z_1(z)$. To obtain the longitudinal component of the electric field the electrodes have to be longitudinally perturbed (quasi-periodically) so that the perturbation of the vertical electrodes is shifted by a period of $\beta\lambda/2$ with respect to the horizontal ones.

Looking at Figure 2 it is clear that the angular function $\Theta_0(\theta)$ has to satisfy only conditions i. and ii. of paragraph 1.2, and it can be written as:

$$\Theta_1(\theta) = \Sigma_n a_n \cos 2n\theta \tag{1.3.1}$$

The function $Z_1(z)$ representing the quasiperiodic variation along the z axis, can be written as a cosine and sinus series:

$$Z_1(z) = \Sigma_m c_m \cos mkz + \Sigma_p d_p \sin pkz \tag{1.3.2}$$

where $k = 2\pi/\beta\lambda$. The first condition on $Z_1(z)$ is a zero slope at the beginning of the period (see Figure 2):

i) $dZ_1(z)/dz|_{z=0} = 0$

which is true only if $d_p = 0 \ \forall p$

We impose now the condition of the shifted longitudinal perturbation:

$$U_1(r,\theta,z) = - U_1(r, \theta \pm \pi/2, \beta\lambda/2 - z) \tag{1.3.3}$$

Looking at the expressions of $\Theta_1(\theta)$ and of $Z_1(z)$ we see that Eq.(1.3.3) is satisfied when $\cos n\pi \cos m\pi = -1$ that is, if the sum of n and m is an odd number.

The Laplace equation, written in cylindrical coordinates, is:

$$\Theta_1(\theta)Z_1(z)\partial^2R_1(r)/\partial r^2 + (1/r)\Theta_1(\theta)Z_1(z)\partial R_1(r)/\partial r$$

$$+ (1/r^2)R_1(r)Z_1(z)\partial^2\Theta_1(\theta)/\partial\theta^2 + R_1(r)\Theta_1(\theta)\partial^2Z_1(z)/\partial z^2 = 0 \tag{1.3.4}$$

Inserting now the functions $\Theta_1(\theta)$ and $Z_1(z)$ and performing their respective derivatives in θ and z we obtain an expression for the function R(r):

$$\Sigma_n\Sigma_m \cos2(2n+1)\theta \cos mkz \cdot$$

$$\cdot[r^2\partial^2R_1(r)/\partial r^2 + r\partial R_1(r)/\partial r - (m^2k^2r^2 + 4n^2)R_1(r)] = 0 \tag{1.3.5}$$

Inside the square brackets we recognize the differential equation satisfied by the modified Bessel function of argument mkr and order 2n. The potential function U can be written finally as:

$$U(r,\theta,z) = (V/2)\Sigma_p A_{0\,2p+1} r^{2(2p+1)} \cos2(2p+1)\theta$$

$$+ (V/2)\Sigma_n\Sigma_m A_{mn} I_{2n}(mkr) \cos2n\theta \cos mkz \tag{1.3.6}$$

with $n+m = 2p+1$ $(p = 0,1,2,...)$. V is the potential difference between two vanes; when the two horizontal electrodes are at potential V/2, the vertical ones are at $-V/2$ and viceversa.

1.4 First order potential function and fields.

Usually only the first two terms of equation (1.3.6) are considered as a good approximation to start with [3] and the potential function is:

$$U(r,\theta,z) = V/2\cdot(A_{01} r^2 \cos2\theta + A_{10} I_0(kr) \cos kz) \tag{1.4.1}$$

Eqs.(1.3.6) and (1.4.1) refer to one unit cell. The coefficients Aij change from cell to cell. Their variation determines the characteristics of the accelerator.

It is usual to call 'a' the minimum distance of the vane to the axis in one cell, and 'ma' the maximum one, 'm' being the modulation factor (see Figure 1).

From equation (1.4.1), as $U(a,0,0) = U(ma,0,\beta\lambda/2) = V/2$, it is easy to write the relationship between Aij and the geometrical parameters ('a','m') of the cell:

$$A_{10} = \frac{m^2 - 1}{m^2 I_0(ka) + I_0(mka)} \tag{1.4.2}$$

$$A_{01} = (1/a^2)[1 - A_{10}\, I_0(ka)] \tag{1.4.3}$$

The components of the electric field are derived from (1.4.1):

$$E_r = -\partial U/\partial r = -V/2\cdot[\, 2A_{01}\, r \cos 2\theta + kA_{10}\, I_1(kr) \cos kz\,] \tag{1.4.4}$$

$$E_\theta = -\, 1/r\, \partial U/\partial\theta = VA_{01}\, r \sin 2\theta \tag{1.4.5}$$

$$E_z = -\partial U/\partial z = kV/2\, A_{10}\, I_0(kr) \sin kz \tag{1.4.6}$$

Other usual definition in the RFQ literature is the focusing force factor B:

$$B = (q/m_0c^2)\lambda^2(\chi V/a^2) \tag{1.4.7}$$

where χ is

$$\chi = \frac{I_0(ka) + I_0(mka)}{m^2 I_0(ka) + I_0(mka)} \tag{1.4.8}$$

A_{10} and χ are related by:

$$A_{10} I_0(ka) + \chi = 1 \tag{1.4.9}$$

The mean aperture of the vanes r_0 is (see Figure 1):

$$r_0 = 1/\sqrt{A_{01}} = a\sqrt{\chi} \tag{1.4.10}$$

1.5 Multipolar expansion of the potential function and fields.

The lowest terms potential of Eq.(1.4.1) specifies equipotential surfaces whose transverse sections are hiperbolae. The real electrodes are ,however, usually machined either along transverse circular pathes or with a tool whose transverse section is a circle and then cuts elliptical sections (see Chapter 4).

A more exact representation of the real electrodes requires a potential function with multipole terms, whose coefficients can be determined analitycally or numerically.

A good approximation which permits to describe the transverse circular shape of the vanes in the region near the axis (see Appendix A) is a function where octupole and duodecapole tems are added:

$$U(r,\theta,z) = (V/2)\{(A_{01}r^2 \cos 2\theta + A_{03}r^6 \cos 6\theta) + [A_{10}I_0(kr) + A_{12}\cos 4\theta\, I_4(kr)]\, \cos kz\} \tag{1.5.1}$$

Analytically the coefficients are computed imposing boundary conditions (see Appendix A) for each cell of the RFQ.

The components of the electric field are now:

$$E_r = -(V/2)\{2A_{01}r\,[\cos 2\theta + 3\alpha_{13}r^4\cos 6\theta] + A_{10}\,[kI_1(kr) + \beta_{12}\cos 4\theta\,\partial I_4(kr)/\partial r]\,\cos kz\} \quad (1.5.2)$$

$$E_\theta = V\,\{A_{01}r\,[\sin 2\theta + 3\alpha_{13}r^4\sin 6\theta] + 2A_{12}\sin 4\theta\,I_4(kr)\,\cos kz\} \quad (1.5.3)$$

$$E_z = (V/2)kA_{10}\,[I_0(kr) + \beta_{12}\cos 4\theta\,I_4(kr)]\,\sin kz \quad (1.5.4)$$

where $\alpha_{13} = A_{03}/A_{01}$ and $\beta_{12} = A_{12}/A_{10}$.

2. SECTIONS OF THE RFQ

The beam inside the accelerator undergoes the transformation from continous to bunched, and the action of the RFQ on the beam must be adapted to the specific requirements of the particle dynamics during the transport along the structure. So the RFQ is usually divided into sections, distinguished one from the other by the different tasks they fulfill.

In our design we follow the Los Alamos description [3] The sections are:

. Radial Matching Section (RMS)
. Shaper
. Gentle Buncher
. Accelerating Section

We dedicate now a paragraph to each section, marking out its main characteristics.

2.1 Radial Matching Section (RMS)

The RFQ receives normally a continous beam, which comes from a time independent focusing channel. The fields in the RFQ are time dependent and so are the matching conditions. The task of the RMS is to match the beam, at all instants, to the time varying fields.

Several RMS have been proposed [5] [6] [7] and we will describe the one we have included in the design of the RFQ2 and which was first introduced by Crandall [5] : the idea is to start with a very weak focusing at the beginning of the RMS and increase it progressively towards the end. If this is properly done, it is amazing how well the beam is matched at the end of the RMS. To achieve a gradual focusing, the vane aperture starts with a large value and becomes nominal only at the end of the RMS (see Figure 3). The potential function which describes the equipotential surfaces is obtained from the Laplace equation, as we have seen in the previous chapter. We will call now this function $U_2 = R_2(r)\Theta_2(\theta)Z_2(z)$ and apply to it the conditions appropiate to the RMS section.

The exact quadrupolar symmetry is the only condition on the angular variable. So the function $\Theta_2(\theta)$ is equal to $\Theta(\theta)$ given in Eq.(1.2.3).

The function $Z_2(z)$ can be written as before as a sine and cosine series:

$$Z_2(z) = \Sigma_m \alpha_m \sin mKz + \Sigma_p \beta_p \cos pKz \qquad (2.1.1)$$

where the constant K is related to the length L_{RMS} of the RMS section : $K = \pi/2L_{RMS}$

The vanetip profile must have a zero slope at $z = L_{RMS}$; so $\partial Z_2(z)/\partial z|_{z=L_{RMS}} = 0$, which is satisfied only if $\beta_p = 0\ \forall p$ and if m is odd.

To obtain $R_2(r)$ we proceed as before. Substituting $\Theta_2(\theta)$ and $Z_2(z)$ into the Laplace equation, we are left with the following differential equation:

$$\Sigma_{nm}\{ r^2\partial^2 R_2(r)/\partial r^2 + r\partial R_2(r)/\partial r - [4(2n+1)^2 + K^2(2m+1)^2 r^2]\} = 0 \qquad (2.1.3)$$

whose solution is the Bessel series

$$R_2(r) = \Sigma_{mn}\gamma_{mn}I_{2(2n+1)}[(2m+1)Kr] \tag{2.1.4}$$

The potential in the RMS is then:

$$U_2(r,\theta,z) = (V/2)\Sigma_{mn}A_{mn}I_{2(2n+1)}[(2m+1)Kr]\cos2(2n+1)\theta\ \sin[(2m+1)Kr] \tag{2.1.5}$$

From the infinite series we take only the lowest order terms, and we drop the subindex in U:

$$U(r,\theta,z) = V/2\ [\ Q(r,z)\cos2\theta + D(r,z)\cos6\theta\ ] \tag{2.1.6}$$

being Q(r,z) the factor in r and z of the quadrupolar term:

$$Q(r,z) = A_{00}\ I_2(Kr)\ \sin Kz + A_{10}\ I_2(3Kr)\ \sin3Kz \tag{2.1.7}$$

and D(r,z) of the duodecapolar term:

$$D(r,z) = A_{01}\ I_6(Kr)\ \cos Kz + A_{11}\ I_6(3Kr)\ \sin3Kz \tag{2.1.8}$$

The coefficients are determined from the following boundary conditions:
i) The longitudinal field must be zero at the entrance of the RMS section.
ii) The potential must be V/2 on the vane surface.
iii) The transverse radius of curvature of the surface at the vane tip, $\rho(r,0,z)$, is equal to a given value ρ_0.

The corresponding equations are:

i) $\partial U/\partial z = 0$ at $z = 0$

From $\partial Q/\partial r = \partial D/\partial r = 0$ the relationships between A_{00} and A_{10} and between A_{01} and A_{11} follow:

$$\begin{aligned} A_{10} &= -A_{00}/3^3 \\ A_{11} &= -A_{01}/3^7 \end{aligned} \tag{2.1.9}$$

(we have used the approximation of the modified Bessel functions for small arguments: $I_n(x) \approx x^n/(2^n n!)$ and we have neglected the terms of higher order in r)

ii) $U(r_0,0,L_{RMS}) = V/2$

iii) $\rho(r_0,0,L_{RMS}) = \rho_0$

where r_0 is the distance between the vane and the axis at $z = L_{RMS}$.

Solving the system defined by these two last equations (see Appendix B), we can write the electric potential as follows:

$$U(r,\theta,z) = V/2\ [\ A_q\ q(r,z)\cos2\theta + A_d\ d(r,z)\cos6\theta\ ] \tag{2.1.10}$$

where q(r,z) and d(r,z) are:

$$\begin{aligned} q(r,z) &= I_2(Kr)\sin Kz - 1/3^3\ I_2(3Kr)\sin3Kz \\ d(r,z) &= I_6(Kr)\sin Kz - 1/3^7\ I_6(3Kr)\sin3Kz \end{aligned} \tag{2.1.11}$$

and the coefficients A_q and A_d are determined by the aperture r_0, the value of the transverse radius of curvature ρ_0 and the total length L_{RMS} (see Appendix B).

The equipotential surface which defines the shape of the electrodes satisfies the equation:

$$A_q\, q(r,z)\cos 2\theta + A_d\, d(r,z)\cos 6\theta = \pm 1 \tag{2.1.12}$$

The vane profile along z, obtained from (2.1.12) when $\theta = 0$ is represented in Figure 3 together with the variation of $\rho(r,0,z)$ (see Appendix B):

$$\rho(r,0,z) = \frac{r^2}{r - \partial^2 r/\partial\theta^2} \tag{2.1.13}$$

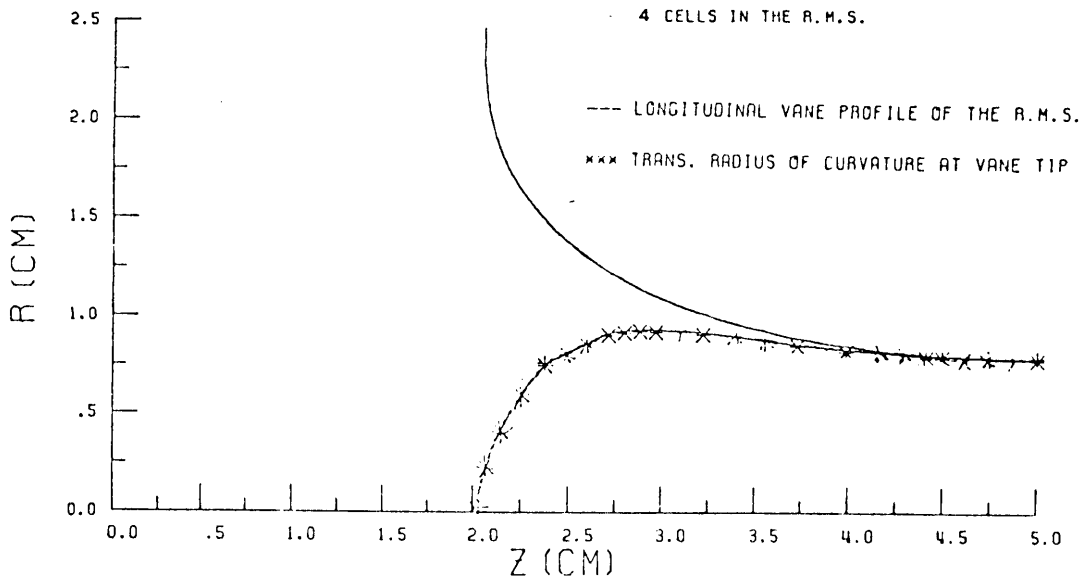

Figure 3: Radial Matching Section

The transverse matching in the RMS requires the focusing force to pass slowly from zero to the final value of B_f at $z = L_{RMS}$, which is $B_f = (32/3)VK^2A_q$.

The radial field near the axis is:

$$E_r = -\partial U/\partial r \approx -V/8\, K^2 A_q r\,(\sin Kz - 1/3\, \sin 3Kz) \tag{2.1.14}$$

The focusing force constant is

$$B(z) = \partial E_r/\partial r \approx V/8\, K^2 A_q\,(\sin Kz - 1/3\, \sin 3Kz) \tag{2.1.15}$$

which gives $B(L_{RMS}) = B_f$. The smooth transition between the RMS and the next section is thus insured (see Figure 4).

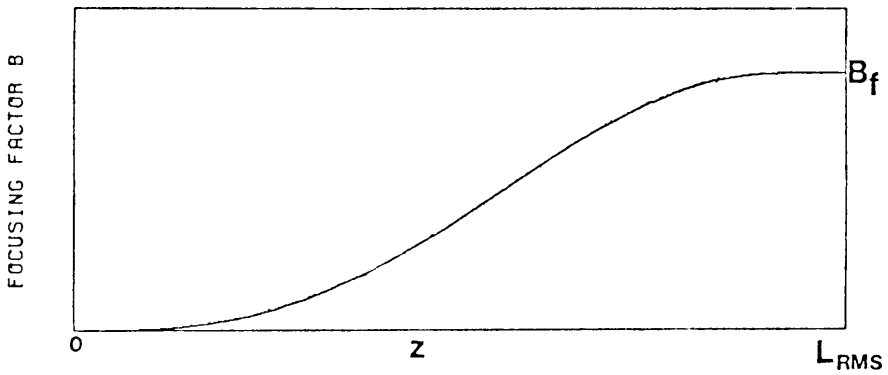

Figure 4: Focusing force factor in the RMS

2.2 Shaper

When Kapchinskii proposed the acceleration by an rf quadrupole [8] he emphasized the importance of keeping constant the shape of the longitudinal emittance, by imposing the constancy of the bunch length and of the frequency of the small oscillations. These conditions can be satisfied only when the longitudinal emittance is finite, i.e. when the beam is bunched. This is not the case of a beam coming from the source and having no longitudinal structure at all. Therefore a section is needed in the RFQ to change, in a smooth way, the longitudinal phase space, by rearranging the particles coordinates and starting to create the longitudinal emittance. This can be obtained by increasing slowly the accelerating factor A_{10} and the synchronous phase ψ_s , which starts at -90^0. The beam will be accelerated by a small amount and will start to get bunched.

We describe now the equations which characterize the Shaper.

The variation of the energy W of a particle of charge q and phase ψ is

$$dW/dz = qETcos\psi = (qA_{10}V/\beta\lambda)(\pi/2)cos\psi \qquad (2.2.1)$$

where ET is the mean longitudinal electric field on axis multiplied by the transit time factor (which, in the RFQ, is $\pi/4$ [3]). The variation of β in nonrelativistic approximation is then:

$$d\beta/dz = (\pi/2)(qV/mc^2\lambda)A_{10}cos\psi/\beta^2 \qquad (2.2.2)$$

We consider now the synchronous particle ($W = W_s$, $\psi = \psi_s$), and we look at the laws of variation of A_{10} and ψ_s . They can be chosen in several ways, providing that a smooth variation is kept. We describe the method, which is used at LANL:

Accelerating factor A_{10}.

It is varied linearly with z

$$A(z) = (A_{sh}/L_{sh})z \qquad (2.2.3)$$

L_{sh} is the length of the Shaper and A_{sh} the value of A_{10} at the end of the section.

Synchronous phase.

The synchronous phase and the separatrix length Φ_s are related by (see Figure 5):

$$tg\psi_s = \frac{\sin\Phi_s - \Phi_s}{1-\cos\Phi_s} \tag{2.2.4}$$

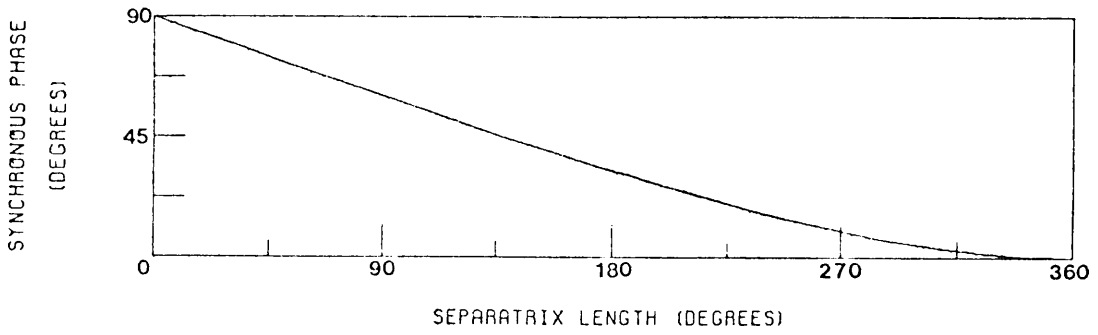

Figure 5: Separatrix length versus synchronous phase

We have considered two possibilities:

a. Linear variation of ψ_s, from which the variation of Φ_s follows according to eq.(2.2.4)

$$\psi_s = \psi_{si} + \Delta\psi(z-z_0)/(L_{sh}-z_0); \tag{2.2.5}$$

ψ_{si} is the initial synchronous phase (normally equal to $-\pi/2$). $\Delta\psi$ is the increase in synchronous phase along the Shaper

$$\Delta\psi = \psi_{sh} - \psi_i = \psi_{sh} + \pi/2 \tag{2.2.6}$$

and z_0 is an initial fraction of the Shaper where ψ_s is kept constant.

b. Linear variation of Φ_s and related variation of ψ_s

$$\Phi_s = \Phi_{si} + \Delta\Phi_s(z-z_0)/(L_{sh}-z_0) \tag{2.2.7}$$

where the parameters are the analogous of those of Equation (2.2.5) In this case the beam is more stable but the total length of the section increases. The difference is anyhow very small.

Length

The length of the shaper, L_{sh}, can be obtained by integrating the equation (2.2.2); one can proceed as follows:

a. Substituting Eqs. (2.2.3) and (2.2.5) into (2.2.2) and rearranging the terms, we obtain:

$$\int_0^{L_{sh}} (A_{sh}/L_{sh})\, z \sin[\Delta\psi(z-z_0)/L_{sh}]dz = (2/\pi)(mc^2\lambda/qV) \int_{\beta_i}^{\beta_{sh}} \beta^2 d\beta \qquad (2.2.8)$$

from where

$$L_{sh} = 2mc^2\lambda(\beta^3_{sh} - \beta^3_i)F/(3\pi qVA_{sh}) \qquad (2.2.9)$$

with

$$F = (\Delta\psi)^2/(1-\Lambda)[\Lambda\Delta\psi - \Delta\psi\cos\Delta\psi + (1-\Lambda)\sin\Delta\psi] \qquad (2.2.10)$$

and $\Lambda = z_0/L_{sh}$

b. The length Lsh is obtained by the numerical integration of Eq.(2.2.2).

2.3 Gentle Buncher.

After the Shaper, Kapchinskii's laws [1] can be applied to the already bunched beam. LANL calls this section the Gentle Buncher and it corresponds in fact to Kapchinskii's original proposal.

The longitudinal characteristics of the bunch are manteined by keeping constant:

- frequency of the oscillations: $A_{10}\sin\psi_s/\beta^2 = C_1$ (2.3.1)
- bunch length : $\beta\Phi_s = C_2$ (2.3.2)

Given the values of A_{10}, ψ_s and of the energy at the end of the section and one of them at the beginning, the whole set of parameters is completely determined in the Gentle Buncher.

The length of the section is obtained analogously to the previous case: integrating

$$d\beta = (\pi/2)(qV/mc^2\lambda)(A_{10}\sin\psi_s/\beta^2)\cot g\psi_s\, dz \qquad (2.3.3)$$

the length is

$$L_{gb} = (2mc^2\lambda/\pi qVC_1) \int_{\beta_{sh}}^{\beta_{gb}} tg\psi_s(\beta)\, d\beta \qquad (2.3.4)$$

2.4 Accelerating section.

The values of 'a' and 'm' are kept constant. The beam is well bunched when it gets into the Accelerating Section, and normally the synchronous phase is not modified inside the section.

The accelerating factor can be approximated by:

$$A_{10} \approx \frac{m^2 - 1}{m^2 + 1 + 2\pi^2 m^2 a^2/(\beta\lambda)^2} \tag{2.4.1}$$

Integrating as usual between the beginning and the end of the section

$$(\beta^2/A_{10})\, d\beta = C \cos\psi_s\, dz \tag{2.4.2}$$

where $C = \pi qV/(mc^2\lambda)$, the length can be written as:

$$L_{as} = A_\beta / C A_\psi \tag{2.4.3}$$

with

$$A_\beta = (\beta^3_f - \beta^3_{gb})/3 + (2\pi/\lambda)^2 m^2 a^2 (\beta_f - \beta_{gb})/(m^2 - 1) \tag{2.4.4}$$

and

$$A_\psi = \begin{cases} \cos\psi_f & \text{if } \psi_{gb} = \psi_f \\ (\sin p\psi_f - \sin\psi_{gb})/(\psi_f - \psi_{gb}) & \text{if } \psi_{gb} \neq \psi_f \end{cases} \tag{2.4.5}$$

In the accelerating section we have a phase damping given with

$$\psi_{2s}/\psi_{1s} = (\beta_1/\beta_2)^{1/2} \tag{2.4.6}$$

If the final ψ_s is imposed, this damping has to be taken into account when specifying ψ_s at the end of the Gentle Buncher.

3. SPACE CHARGE AND BEAM CURRENT LIMITS

The motion of the particles inside the accelerator can be dominated by the space charge forces, if the intensity of the beam is sufficiently high. Although a correct presentation of the problem can be presently obtained only by numerical simulation of the particle dynamics, it is however possible to get an idea of the equilibrium between the external and the space charge forces by analytical methods. We use the linear approximation, which is a reasonably correct representation of the transverse plane, while for the longitudinal plane it will give only an indication on the real behaviour of particles, because of the neglection of the strong longitudinal non – linearities and asymmetries.

3.1 Forces acting on particles in the absence of space charge.

We represent the bunch by a three dimensional ellipsoid with uniform charge distribution, whose dimensions are averaged over a focusing period [9]

In the absence of space charge the dynamics of the particles is determined only by the external forces generated by the fields of the structure.

Let's consider a bunch of particles (rest mass m_0 and charge q) injected in an RFQ working at frequency f ($f = c/\lambda$) and intervane voltage V. In one cell of the structure, with minimum aperture 'a' and maximum aperture 'ma', the focusing forces acting on the particles are given, in the normalized system, by the square of the phase advances per period, σ_{0t} and σ_{0l} [13.] where the subindex stay for transverse and longitudinal, respectively:

$$\sigma^2_{0t} = B^2/(8\pi^2) + \Delta_{rf} \tag{3.1.1}$$

$$\sigma^2_{0l} = -2\Delta_{rf} \tag{3.1.2}$$

B is the focusing factor already introduced in the previous chapter, constant along the structure if the mean radius of aperture, r_0, is constant. Δ_{rf} is the rf factor, defocusing in both transverse planes and focusing in the longitudinal one:

$$\Delta_{rf} = (\pi^2 q/2m_0c^2)(\sin\psi_s/\beta^2)A_{10}V \tag{3.1.3}$$

3.2 Forces acting on particles with space charge.

When the space charge forces are not negligible, the focusing strengths are diminished by a factor $\mu_{t,l}$ (transverse and longitudinal space charge factor, respectively):

$$\sigma^2_{t,l} = \sigma^2_{0t,l}(1 - \mu_{t,l}) \tag{3.2.1}$$

where $\mu_{t,l}$ is given by:

$$\mu_{t,l} = \Delta_{sct,l}/\sigma^2_{0t,l} \tag{3.2.2}$$

$\Delta_{sct,l}$ is the space charge force (see later). We assume that the mean radius of the bunch is the geometric mean of the maximum and minimum semiaxes over a focusing period [9] :

$$r = \sqrt{(\lambda E_n/\sigma_t)} = r^0/(1-\mu_t)^{1/4} \tag{3.2.3}$$

where E_n is the normalized transverse emittance and r^0 is the mean radius of the bunch in absence of space charge forces ($r^0 = \sqrt{(\lambda E_n/\sigma_{0t})}$).

Increasing the current the beam transverse dimensions increase and the maximum allowed r is limited by the value of the minimum aperture a:

$$r_{max} = a/\sqrt{\Psi} \tag{3.2.4}$$

where Ψ is the average modulation factor

$$\Psi = \sqrt{(\beta_+/\beta_-)} \approx \frac{1+B/(4\pi^2)}{1-B/(4\pi^2)} \tag{3.2.5}$$

in the reasonable hypothesis $\Delta_{rf} \ll B^2$; $\beta_{+,-}$ are the maximum and minimum of the amplitude function respectively.

As the beam current increases, 'a' must be kept always over the value

$$a_{th} = r^0\sqrt{\Psi}(1-\mu_t)^{-1/4} \tag{3.2.6}$$

The half longitudinal dimension of the bunch is [10] :

$$b = (3\beta\lambda/4\pi)|\psi_s|(1-\mu_l) \tag{3.2.7}$$

3.3 Equilibrium between external and space charge forces.

In the RFQ the smallest effective value of the aperture 'a' occurs in the Accelerating Section. The most critical point in the transverse plane is then the end of the Gentle Buncher, because there the defocusing force Δ_{rf} is higher than in the following section ($\Delta_{rf} \propto \beta^{-2}$), while the aperture is the same. From now on we will refer the studies of this chapter to this point, and we suppose that, if the beam can be transported through it, it will also be stable along the whole accelerator. This assumption has proved to be valid by numerical simulation of particle behaviour in the RFQ.

We have seen that the current transported in the accelerator decreases the focusing efficiency of the system and the frequency of the particle oscillations. Appropiate values of σ_{0t} and σ_{0l} must be chosen in order to obtain the desired values of σ_t and σ_l in the presence of space charge.

We inverte formally the problem: given σ_{0t} and σ_{0l} we calculate the corresponding parameters of the RFQ (tension V, focusing force, accelerating factor) for a certain current.

From equations (3.1.1) through (3.1.3) we can write:

$$A_{10}V = (m_0c^2/\pi^2q)(\beta^2/\sin\psi_s)\sigma^2{}_{0l} = A_l \tag{3.3.1}$$

$$S_\sigma = (\sigma^2{}_{0t} + \sigma^2{}_{0l}/2)^{1/2} \tag{3.3.2}$$

$$\chi V/a^2 = 2\sqrt{2\pi}(m_0c^2/q)(1/\lambda^2)\,S_\sigma = A_t \tag{3.3.3}$$

$$\Psi = (\pi\sqrt{2} + S_\sigma)/(\pi\sqrt{2} - S_\sigma) \tag{3.3.4}$$

The values of A_t and A_l depend only on σ_{0t} and σ_{0l} if the synchronous phase and energy are given. Multiplying Eq.(1.4.9) by V, we have:

$$V = A_{10}VI_0(ka) + \chi V = A_lI_0(ka) + A_ta^2 \tag{3.3.5}$$

The accelerating and the focusing factors are:

$$A_{gb} = A_l/V \tag{3.3.6}$$

$$B = 2\sqrt{2S_\sigma} \tag{3.3.7}$$

The 'a' appearing in Eq.(3.3.5) is the real aperture of the vanes, obtained from a_{th} of Eq.(3.2.6) multiplied by a safety factor S_f which takes into account various tolerances ($S_f \approx 1-1.5$).

3.4 Current limits.

Given the values of σ_{0t} and σ_{0l} a current limit exists for each value of μ_t and the corresponding μ_l .

According to the three dimensional ellipsoid model [9] the transverse space charge force is

$$\Delta_{sct} = -[3Z_0qI_t\lambda^3(1-f(p))]/(8\pi m_0c^2r^2b) \tag{3.4.1}$$

where $Z_0 = 1/(\epsilon_0 c)$ is the impedance of free space, $p = b/r$ is the ellipsoid axis ratio and f(p) is the ellipsoid factor [9.]

Substituting r and b with the expressions of Eqs. (3.3.3) and (3.2.7) and utilizing the definition of σ_t , the transverse current limit I_t may be written as:

$$I_t = (2m_0c^2/Z_0q)(\beta|\psi_s|E_n/\lambda)[1/(1-f(p))]\sigma_{0t}\,\mu_t(1-\mu_l)/\sqrt{(1-\mu_t)} \tag{3.4.2}$$

The longitudinal space charge force is, in the smooth approximation [9] :

$$\Delta_{scl} = -[3Z_0qI_l\lambda^3f(p)]/(4\pi m_0c^2r^2b) \tag{3.4.3}$$

from where

$$I_l = (m_0c^2/Z_0q)(\beta|\psi_s|E_n/\lambda)(1/f(p))(\sigma^2{}_{0l}/\sigma_{0t})(1-\mu_l)\mu_l/\sqrt{(1-\mu_t)} \tag{3.4.4}$$

Writing the space charge forces in function of the charge density ($\rho_c = 3I\lambda/(4\pi r^2bc)$) instead of the current intensities, we can relate the longitudinal and the transverse space charge factors by

$$\mu_l = [2f(p)/(1-f(p)](\sigma_{0t}/\sigma_{0l})^2\,\mu_t \tag{3.4.5}$$

A necessary condition for stability is that both μ_t and μ_l are less than unity.

In the following figures 6,7, the relationship between the space charge factors, the current limits and the bunch dimensions are illustrated. In the transverse plane the behaviour is regular:

the current limit increases with μ_t and so does the bunch mean radius r (Figures 6,7). In the longitudinal plane there exists an optimum value of μ_l ($\mu_l \approx .42$), which corresponds to the maximum longitudinal current (Figures 6,7). This μ_l can be deduced also from Eq.(3.4.4), imposing $dI_l/d\mu_l = 0$. The derivative can be done by numerical methods, because the dependence on μ_l of f(p) and of μ_t must be taken in into account. The longitudinal zone of stability b decreases as the space charge force increases (see Figure 7).

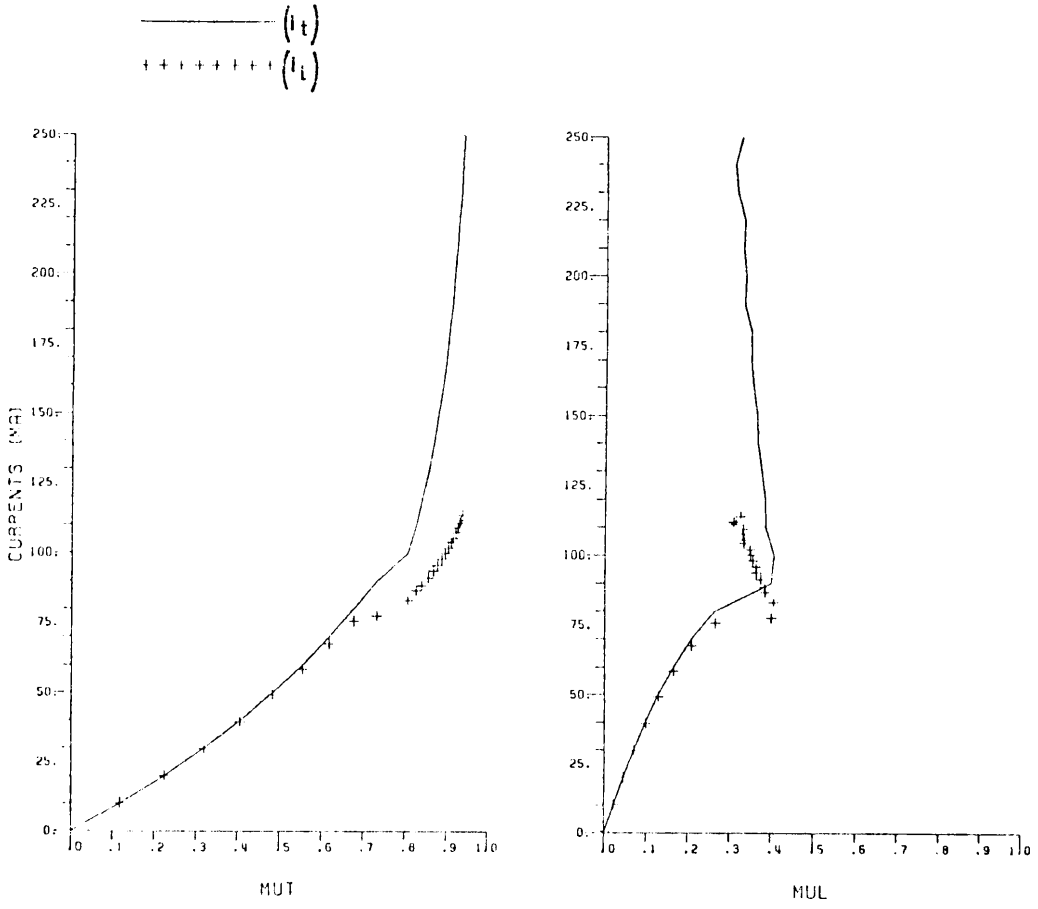

Figure 6: Current limits as functions of space charge factors μ_t, μ_l

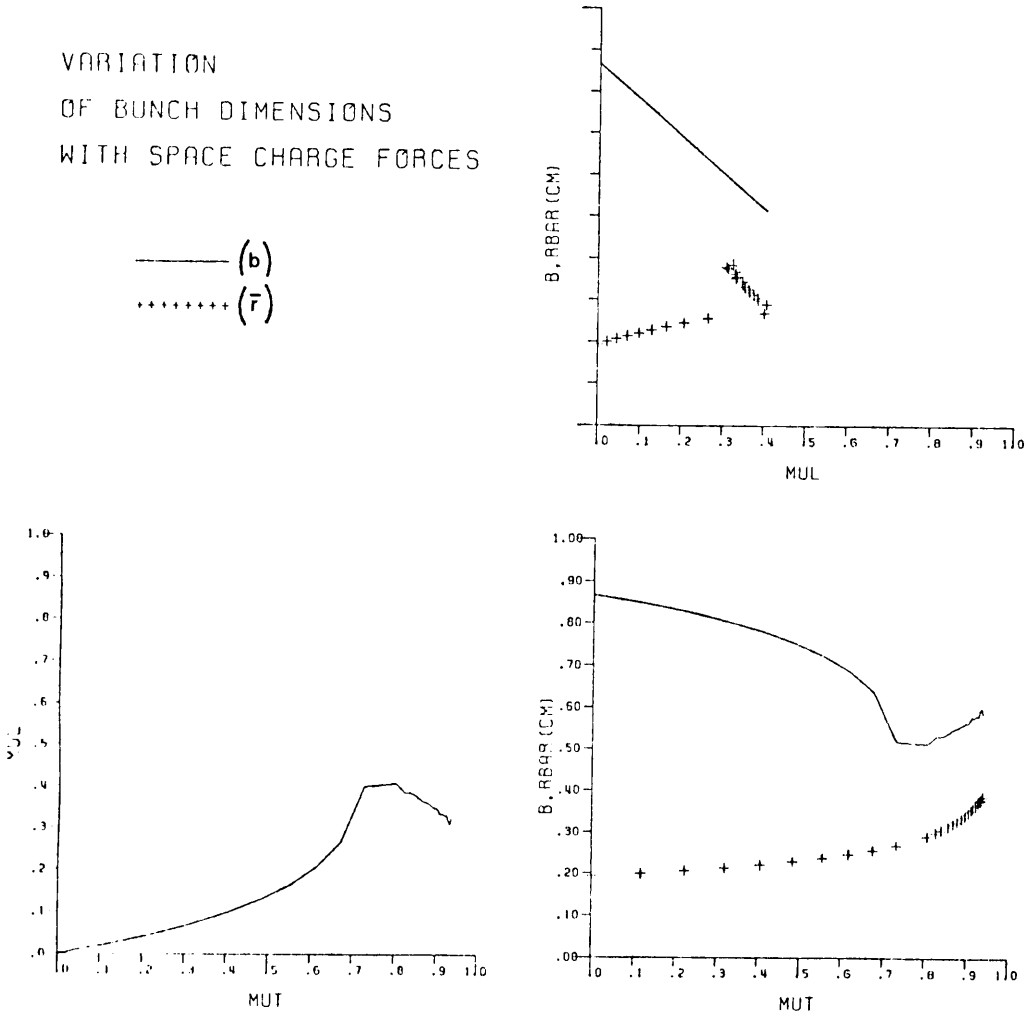

Figure 7: Bunch dimensions

4. DESIGN OF THE RFQ ACCELERATOR

A group of computer codes is now available at CERN (PS division, LINAC group) to study and design an RFQ accelerator. We will give an overview of all of them, illustrating them with the example of the RFQ2 project.

4.1 Choice of σ_{0t}, σ_{0l} (program INPAR).

Our approach in the design of a high intensity RFQ starts with the choice of the phase advances per period at the end of the Gentle Buncher, choice which, as seen in the preceeding chapter, gives the starting values for the tension and the accelerating and focusing factors at this critical point of the accelerator.

The following considerations must be taken into account:

. The current limits are proportional to σ_{0t} and σ_{0l} (see Eqs.(3.4.2/3.4.4)), so high values are required for high intensity beams
. The surface field on vanes must stay in reasonable limits, determined either by the very conservative Kilpatric law [11] or by the value of the product of field and potential, which some consider as the significant figure. This imposes an upper limit on the longitudinal phase advance σ_{0l} to which V is strictly related (see Eq.(3.3.1) and (3.3.5)).
. The energies of oscillation in the transverse and longitudinal plane should be similar, in order to avoid energy transfer between planes, so σ_{0t} and σ_{0l} must be of the same order of magnitude.

The program INPAR (INput PARameters) which compares the bunch size with the aperture in the last cell of the Gentle Buncher and checks the beam stability as the current increases, is used to this purpose. An approximative value of the maximum surface field is also computed, in order to control the breakdown characteristics of the electrodes. An output from the program is given in Table 1 .

4.2 Sections of the accelerator (program RFQIMS).

The following step is the choice of the initial energy W_i, the energy at the end of the Shaper, W_{sh}, and that at the end of the Gentle Buncher, W_{gb}. The following considerations are used as guidelines:

Choice of the initial energy W_i

i. The space charge forces at lower energy increase considerably the transverse dimensions of the beam, which can be critical for the aperture of the LEBT (Low Energy Beam Transport). Normally LEBT contains solenoids to focuse the beam and the total flux of the magnetic field becomes prohibitive at larger aperture.

ii. A lower initial energy is preferable from the point of view of high voltage problems in the preaccelerator.

iii. The length of the RFQ accelerator decreases when the initial energy is higher (see Figure 8).

Choice of W_{sh}.

The Shaper must be long enough to permit a slow bunching of the beam. The synchronous phase must be changed slowly. The value of W_{sh} influences both the length of the accelerator and the efficiency of the structure (see Figure 9 and formula (3.3.9)). The change in the efficiency can be explained with the process of bunching and gradual forming of the longitudinal emittance which is more critical if a higher current must be transported. A compromise between the two different tendencies has to be reached (see always Figure 9).

Choice of W_{gb} and W_f

A reasonable approach is to consider the total increase in energy $(W_f - W_i)$; if it is of the order of $\approx 10W_i$ it is not necessary to use an accelerating section and $W_{gb} = W_f$

Table 1: INPAR output

RO(CM.)= .7013

AV.IO(KA)= .81729E-01 (XV/A..2.).A..2.= .52225E-01

B= 6.4047

PSI= 1.3873 A(CM)= .4379

V(MV)= .13395 AG= .5791

I(MA)= 71.881 AV(MV)= .07757 V.V/A= 4.098

MUT	MUL	SIGMAT	SIGMAL	IT	IL	RBAR	B	FP
.650	.238	20.706	27.066	71.881	71.874	.248	.660	.125
.693	.290	19.385	26.119	81.881	77.277	.256	.615	.142
.746	.434	17.639	23.327	91.881	75.057	.269	.490	.191
.821	.399	14.815	24.027	101.881	84.756	.293	.520	.197
.828	.391	14.532	24.197	111.881	86.157	.296	.528	.196
.845	.385	13.793	24.320	121.881	88.769	.304	.533	.199
.859	.371	13.148	24.588	131.881	91.621	.311	.545	.200
.869	.365	12.650	24.707	141.881	93.635	.317	.550	.202
880	.354	12.112	24.920	151.881	96.042	.324	.560	.203
.889	.355	11.683	24.905	161.881	97.729	.330	.559	.207
.898	.357	11.166	24.857	171.881	99.871	.338	.557	.212
.907	.337	10.686	25.242	181.881	102.462	.345	.574	.210
911	.347	10.465	25.049	191.881	103.412	.349	.566	.216
.919	.346	9.956	25.077	201.881	106.064	.357	.567	.221
.924	.336	9.623	25.253	211.881	107.993	.364	.575	.221
.928	.336	9.367	25.262	221.881	109.482	.369	.575	.224
.933	.311	9.048	25.724	231.881	110.999	.375	.596	.220
.934	.329	8.959	25.392	241.881	111.964	.377	.581	.227

It is also important to consider the intensity of the current: for a very intense bunch the variation of the synchrotron phase must be slow in order to keep the beam stable. So it can be more convenient to lengthen the Gentle Buncher until the end of the accelerator.

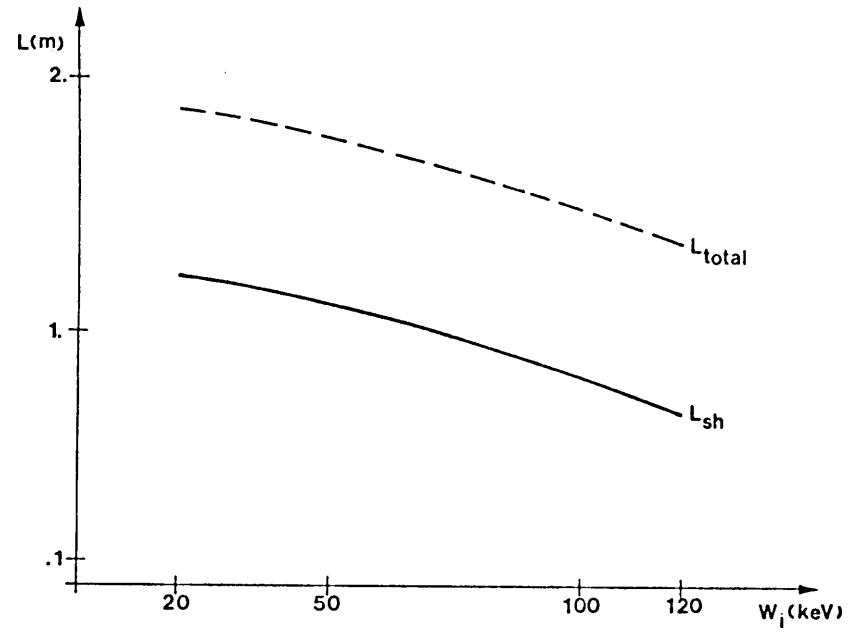

Figure 8: Variation of RFQ length with initial energy $(W_c = 750keV)$

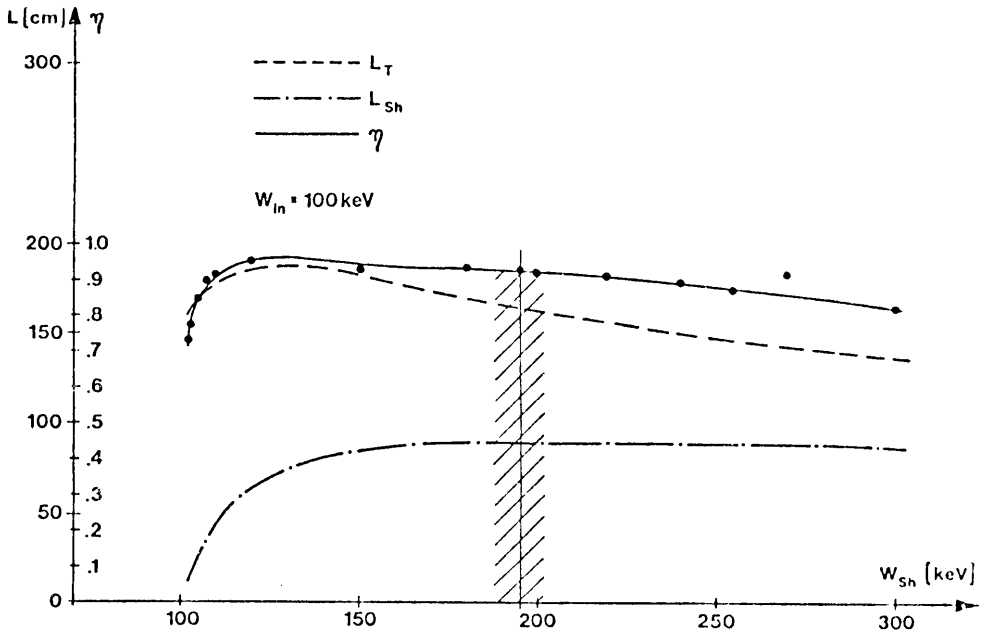

Figure 9: Variation of RFQ length with W_{sh} $(W_f = 750keV)$

If the intensity is not high, the use of the Accelerating Section is preferable because it decreases the length of the accelerator, which means decreasing the costs.

A computer code, RFQIMS, based on the LANL programs RFQUICK and IMS [12] is used to specify the above items. An output of this code is given in Table 2.

Table 2: RFQIMS output

```
**********************************************************************

LR,LS,LG,LA,LT=                      4.      102.      73.       0.      179.
DSC,DRFNL,211/KA,SIGMA =             -.18     -.21      1.31    20.7
PCU,PB,PT(KW)=                     436.5     132.0     568.5

**********************************************************************
```

Z	BB	PHI	M	V	W	AA	A	PSI
-4.100	.200	-90.000	1.000	.170	.090	.000	4.455	360.000
.000	6.400	-90.000	1.000	.170	.090	.000	.787	360.000
1.015	6.400	-90.000	1.002	.170	.090	.001	.787	359.969
26.148	6.400	-83.703	1.058	.170	.092	.019	.766	289.762
51.280	6.400	-77.407	1.103	.170	.107	.037	.751	257.238
76.413	6.400	-71.110	1.126	.170	.142	.055	.743	230.304
101.545	6.400	-64.813	1.139	.170	.200	.073	.738	206.077
113.908	6.400	-59.920	1.161	.170	.239	.092	.730	188.402
123.416	6.400	-55.956	1.186	.170	.279	.112	.722	174.613
131.140	6.400	-52.672	1.214	.170	.318	.133	.713	163.466
137.644	6.400	-49.896	1.244	.170	.357	.155	.703	154.214
143.261	6.400	-47.513	1.276	.170	.396	.178	.692	146.373
148.205	6.400	-45.439	1.311	.170	.436	.203	.681	139.619
152.619	6.400	-43.612	1.349	.170	.475	.229	.670	133.720
156.607	6.400	-41.988	1.390	.170	.514	.255	.658	128.512
160.243	6.400	-40.533	1.434	.170	.554	.283	.645	123.868
163.585	6.400	-39.218	1.482	.170	.593	.311	.631	119.693
166.677	6.400	-38.023	1.534	.170	.632	.341	.617	115.914
169.553	6.400	-36.930	1.591	.170	.671	.371	.603	112.472
172.241	6.400	-35.926	1.653	.170	.711	.402	.587	109.319
174.766	6.400	-35.000	1.721	.170	.750	.434	.571	106.418
174.766	6.400	-35.000	1.721	.170	.750	.434	.571	106.418

4.3 Multipolar potential function (program GENRFQM).

For intense beams, the multipolar components of the electric field in the proximity of the axis can influence sensitively the particle dynamics, and their inclusion in the design of the accelerator is therefore necessary.

Their numerical computation is done by optimization programs which try to fit the equipotential function to the real electrodes. For example the program GENRFQM, which computes the values of the coefficients A_{01}, A_{03}, A_{10} and A_{12} tries to find the best fit at points along RFQ vanes specified by the program RFQIMS.

4.4 Generation of the complete structure. Beam dynamics in the accelerator

(programs PARMTEQ, PARMULT and OUTTEST).

The program PARMTEQ or its derivated version wich icludes the multipole components of the potential function, PARMULT, is used for the generation of the structure cell by cell and for the study of the beam dynamics. For each cell are specified:

- the synchronous energy at the center and at the end of the cell
- the velocity of the synchronous particle
- the mean longitudinal electric field on the axis
- the accelerating factor
- the synchronous phase
- the smallest aperture 'a'
- the modulation factor 'm'
- the rf component of the focusing force
- the cell length
- the ratio A_{03}/A_{01} (if multipoles are included)
- the ratio A_{12}/A_{10} (as before)

An example of the output from PARMULT is given in Table 3

The beam is represented with a distribution of N points in the three phase planes. The coordinates of these points are randomly generated or uniformly positioned in the phase plane ellipses, and followed along the whole structure.

The space charge effects are treated in a special subroutine, SCHEFF. The space charge impulse is imparted to the particles once in each cell, at the position where the beam is roughly circular. The beam is divided in a cylindrical mesh, each point of which is considered as a ring of charge. The field created by the complete mesh on each of its point is computed. The impulse on each particle is obtained computing the field in the position of the particle by interpolation between mesh points, considering the center of the bunch (given by the r.m.s coordinates) as a point charge. The impulse is averaged over $\beta\lambda/2$.

PARMTEQ and PARMULT are completed by another program, OUTTEST, which gives the graphic outputs, all along the RFQ, or in determinates cells. Some examples are given in Figures 10.

Table 3: PARMULT output

```
DESIGN ,FREQ=202.56 MHZ, Q=1.0,WI= .090,WF=  .75 I= 250.0MA,

TANK  1  LENGTH=     180.00 CM,  127 CELLS,  CHARGE STATE  1.

 NC  V       WS    BETA    EZ    CAPA     PHI      A     M      B       CL      TL
  0 .178   .0900 .0138   .000  .00000  -90.0 1.876 1.000    .000
  5 .178   .0900 .0139   .013  .00073  -90.0  .787 1.003  6.687  1.025    5.12
 10 .178   .0901 .0139   .077  .00444  -88.7  .782 1.019  6.687  1.026   10.26
 15 .178   .0904 .0139   .141  .00815  -87.4  .778 1.035  6.687  1.027   15.39
 20 .178   .0908 .0139   .205  .01187  -86.1  .774 1.051  6.687  1.029   20.53
 25 .178   .0917 .0140   .268  .01560  -84.8  .770 1.067  6.687  1.033   25.69
 30 .178   .0930 .0141   .330  .01934  -83.5  .765 1.082  6.687  1.040   30.88
 35 .178   .0949 .0142   .391  .02312  -82.2  .762 1.095  6.687  1.050   36.11
 40 .178   .0976 .0144   .450  .02694  -80.9  .759 1.107  6.687  1.064   41.40
 45 .178   .1011 .0147   .506  .03082  -79.6  .756 1.120  6.687  1.082   46.77
 50 .178   .1057 .0150   .559  .03478  -78.2  .753 1.133  6.687  1.106   52.25
 55 .178   .1114 .0154   .608  .03883  -76.8  .750 1.142  6.687  1.134   57.86
 60 .178   .1184 .0159   .653  .04301  -75.3  .748 1.147  6.687  1.169   63.64
 65 .178   .1270 .0165   .695  .04732  -73.8  .746 1.152  6.687  1.210   69.60
 70 .178   .1372 .0171   .732  .05179  -72.3  .744 1.157  6.687  1.258   75.79
 75 .178   .1495 .0178   .764  .05645  -70.7  .742 1.161  6.687  1.312   82.24
 80 .178   .1639 .0187   .793  .06132  -69.0  .741 1.163  6.687  1.373   88.98
 85 .178   .1807 .0196   .818  .06643  -67.2  .740 1.164  6.687  1.442   96.05
 90 .178   .2004 .0207   .840  .07180  -65.4  .738 1.166  6.687  1.519  103.49
 95 .178   .2241 .0218   .905  .08185  -62.6  .734 1.176  6.687  1.607  111.34
100 .178   .2545 .0233   .988  .09527  -59.2  .729 1.191  6.687  1.712  119.69
105 .178   .2945 .0250  1.106  .11460  -55.5  .720 1.216  6.687  1.841  128.62
110 .178   .3486 .0273  1.271  .14314  -51.4  .708 1.253  6.687  2.001  138.29
115 .178   .4243 .0301  1.498  .18599  -46.9  .689 1.313  6.687  2.205  148.89
120 .178   .5348 .0337  1.833  .25496  -42.0  .658 1.417  6.687  2.471  160.68
125 .178   .7049 .0387  2.358  .37576  -36.8  .600 1.629  6.687  2.831  174.07
127 .178   .7993 .0412  2.621  .44442  -34.6  .566 1.763  6.687  3.012  180.00


NCELL =    0, NGOOD =  180
NCELL =  100, NGOOD =  167
NCELL =  101, NGOOD =  167
NCELL =  102, NGOOD =  167
NCELL =  103, NGOOD =  167
NCELL =  104, NGOOD =  167
NCELL =  105, NGOOD =  167
NCELL =  106, NGOOD =  167
NCELL =  107, NGOOD =  167
NCELL =  108, NGOOD =  167
NCELL =  109, NGOOD =  167
NCELL =  110, NGOOD =  167
NCELL =  111, NGOOD =  167
NCELL =  112, NGOOD =  166
NCELL =  113, NGOOD =  166
NCELL =  114, NGOOD =  165
NCELL =  115, NGOOD =  165
NCELL =  116, NGOOD =  165
NCELL =  117, NGOOD =  164
NCELL =  118, NGOOD =  164
NCELL =  119, NGOOD =  164
NCELL =  120, NGOOD =  164
NCELL =  121, NGOOD =  164
NCELL =  122, NGOOD =  164
NCELL =  123, NGOOD =  164
NCELL =  124, NGOOD =  164
NCELL =  125, NGOOD =  163
NCELL =  126, NGOOD =  160
NCELL =  127, NGOOD =  160
```

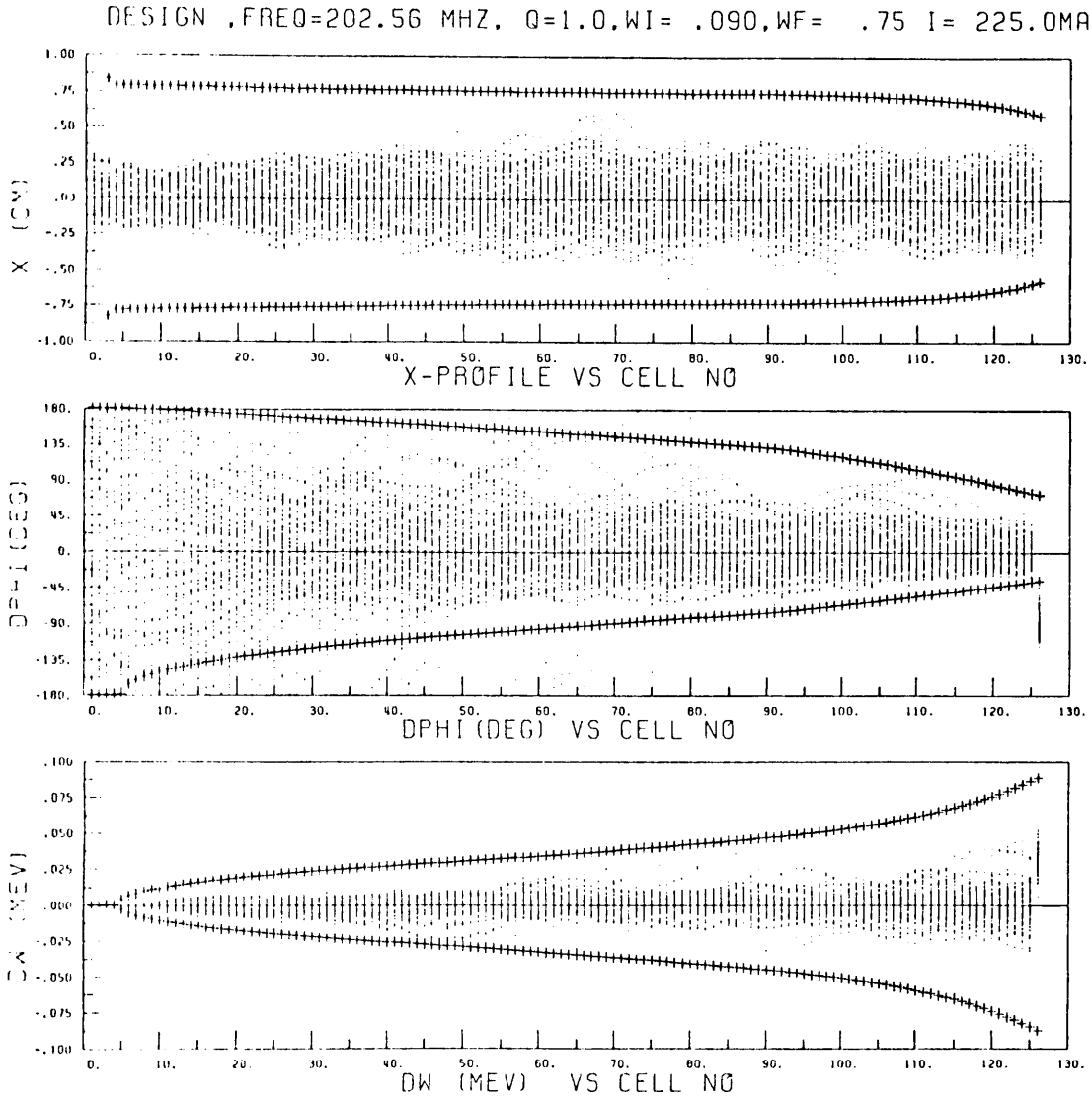

Figure 10: Beam characteristics inside the RFQ2

5. OTHER TOPICS

5.1 Surface fields.

The electric field on the electrode surface is determined by the geometry of the vanes and by the tension applied to them.

A computer program, EFIELD [14] is utilized to check the value reached by the surface electric field, and its distribution along the structure. The region with maximum surface fields is thus found.

The program assumes circular transverse sectioned vanes; the maximum value of the electric field in $z = z_0$ occurs on the axis joining the two centers of curvature of two adjacent vanes. The maximum value in all the RFQ is normally in some point in the Shaper, where the cell length is not high and the modulation factor has already reached values between $1.2 - 1.3$, and it corresponds to the position of the minimum value of the longitudinal radius of curvature.

In Figure 11 the maximum field along the vanes is plotted for the nominal values of the RFQ2.

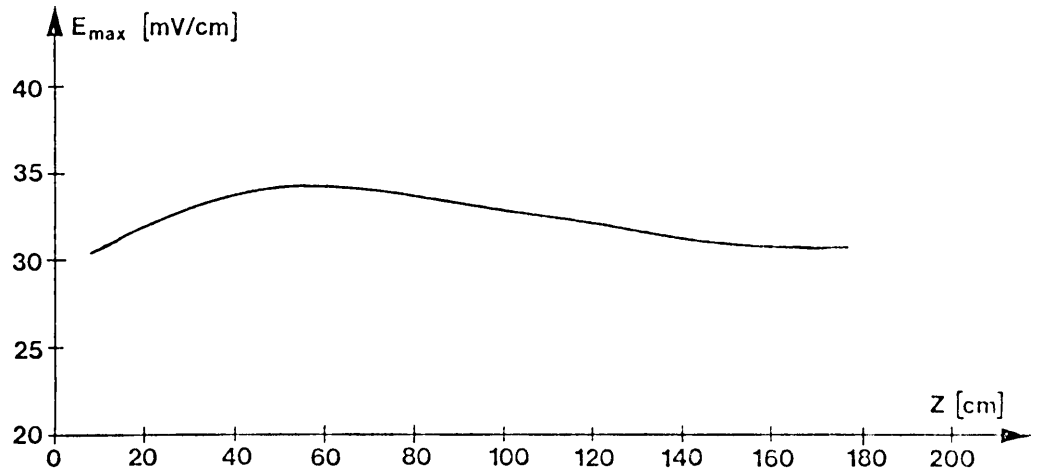

Figure 11: Maximum surface eletric field

5.2 Vane machining

The vanes of the RFQ2 will be machined by a wheel, illustrated in Figure 12, which moves in the longitudinal direction following the vane tip profile. Its transverse section is a circle of radius $R = r_0$. It cuts on the plane normal to the vane tip profile and to the plane $y = 0$ in the point of contact.

The transverse sections of the machined electrodes follow approximately the shape of an ellipse (it would be an exact ellipse if the slope of the electrodes were constant), and they can be computed by the following geometrical considerations.

Let $f(x,z) = 0$ be the equation of the vane tip profile.

$$f(x,z) = A_{01}x^2 + A_{10}I_0(kx)\cos kz \qquad (6.2.1)$$

Let's consider the situation in the instant when the cutter is touching the surface at the point $S = (x_s, 0, z_s)$ (see Figure 13), and check in which point y it cuts the transverse plane $z = z_0$.

The point P, intersection of the normal to the surface at S with the vertical at $z=z_0$, has coordinates $(x_p,0,z_0)$, being

$$x_p = x_s - dz/dx|_s(z_0-z_s) \tag{6.2.2}$$

dz/dx is obtained from Eq.(6.2.1):

$$dz/dx = [2A_{01}x + kA_{10}I_0(kx)\ coskz]/kA_{10}I_0(kx)\ sinkz \tag{6.2.3}$$

The distance s between the points P and S is:

$$s = \sqrt{(z_s-z_0)^2 + (x_s-x_p)^2} \tag{6.2.4}$$

and the y−coordinate of the point Q, contact between the cutter and the surface at $z=z_0$ is

$$y_q = \sqrt{s(2R-s)} \tag{6.2.5}$$

The transverse section of the vane at $z=z_0$ is determined by the consecutive positions of the cutter at A,S,S′,...S^n . Figure 14 illustrates the section in the RFQ where the maximum deviation from a circle occurs. The * correspond to the real machined surface, and the continous line represents a circle. When the slope of the vane tip profile is small, the transverse section is very close to a circle. This is not the case of the Radial Matching Section (see Figure 15). The transverse radius of curvature at the pole tip increases from the value zero corresponding to the beginning of the vane, to the final value ρ_0. We see that the agreement between the machined surface and the theoretical one (continous lines in the figure 15) is better in the first cells of the section. At the end, the machined transverse sections approach a circle, which corresponds to the theoretical circular vane form in the shaper. We should note that, as computed, there is a slight discontinuity between the potential functions at the end of RMS and beginning of shaper; this discontinuity, of course, does not exist on machined vanes.

ACKNOWLEDGEMENTS

During my stage as a fellow at CERN, in the LINAC group of PS division, I have worked in collaboration with M.Weiss. I want to thank him for his continous help and for his discussions and comments on this report.

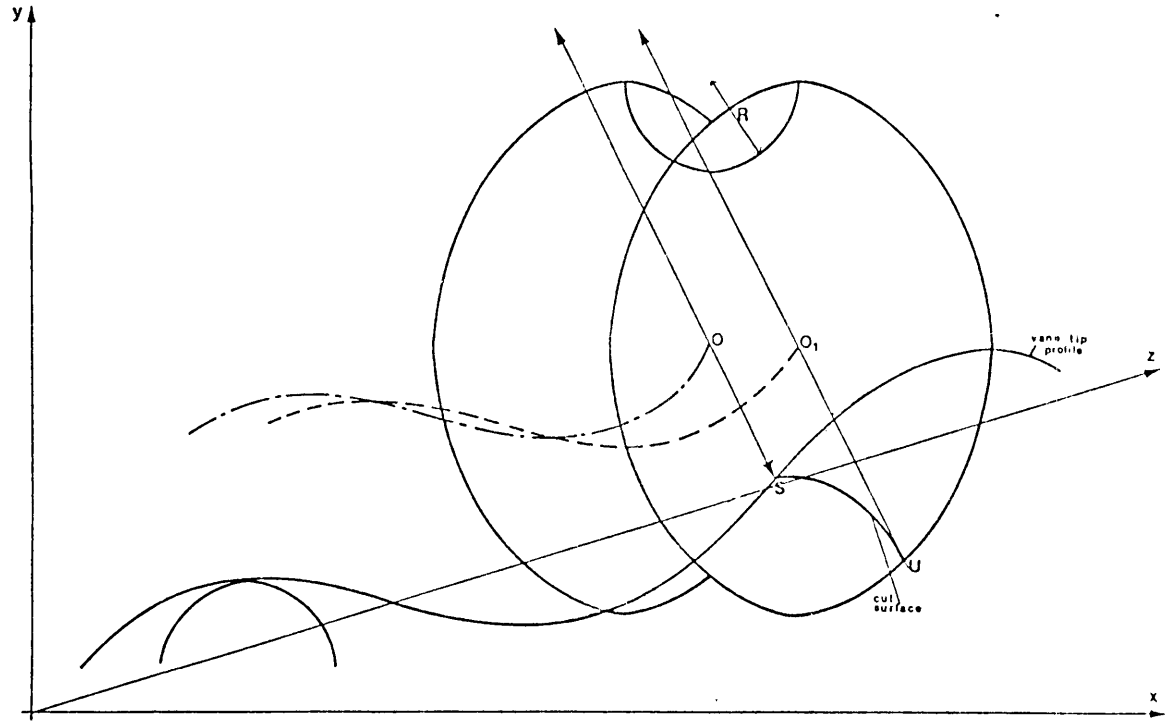

Figure 12: Machining of a vane

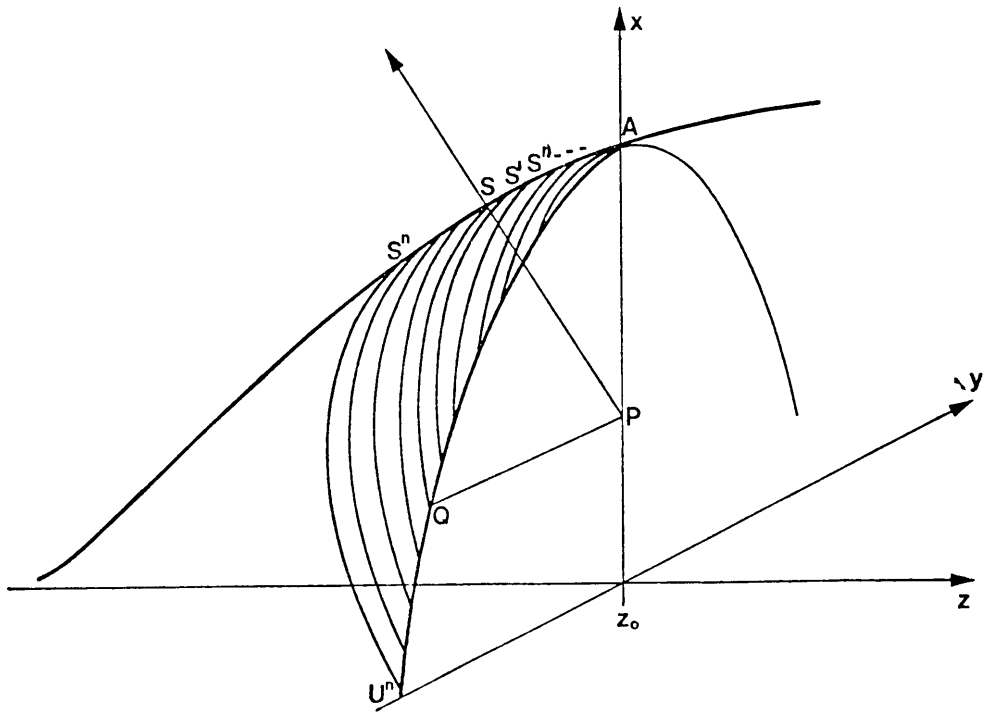

Figure 13: Cutter position

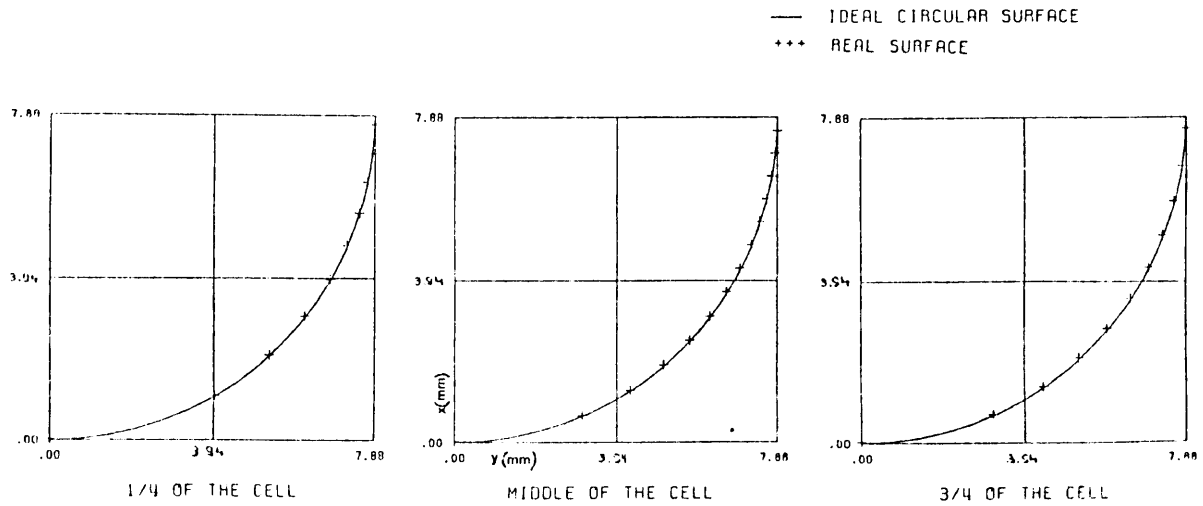

Figure 14: Machined transverse section in a cell of the RFQ2

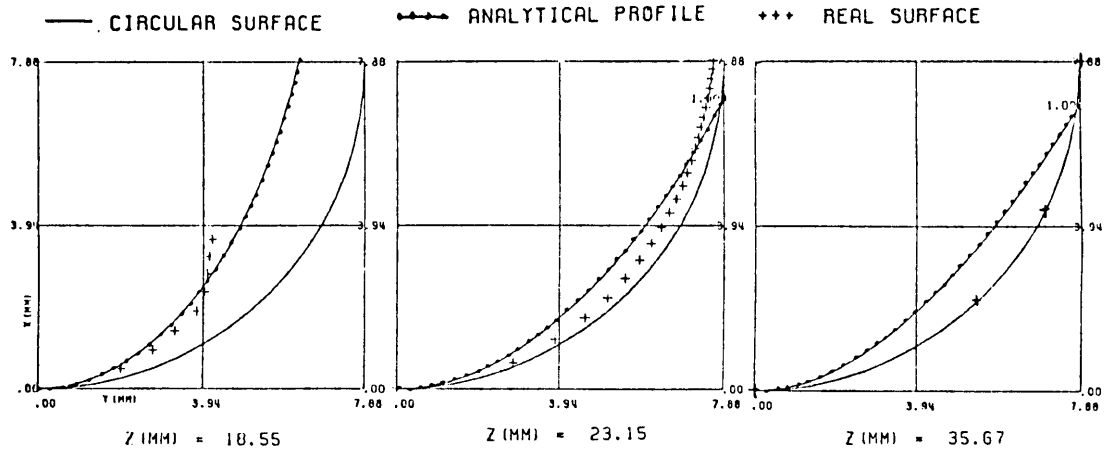

Figure 15: Machined transverse section in RMS

REFERENCES

[1] I.M.Kapchinskyy and V.A.Tepliakov."Linear Ion Accelerator with Spatially Homogenous Strong Focusing" – Prib. Tekh. Eksp., N.2, 19 (1970).

[2] See 'Collection of papers on RFQ Linac' by Accelerator Technology Division Personnel. LANL. November 1980.

[3] K.R.Crandall, R.H.Stokes and T.P.Wangler."RF Quadrupole Beam Dynamics. Design Studies" – Proceedings of the 1979 LINAC Conference.

[4] E.Boltezar et al. "Performance of the CERN RFQ (RFQ1 Project)" – Proceedings of the 1984 LINAC Conference. Seeheim, May 7 – 11 1984.

[5] K.R.Crandall."Proposal for a New RMS for RFQ LINACS" – Internal note LANL. January 1983.

[6] J.L.Laclare and A.Ropert."The SACLAY RFQ" – Saclay Internal Report, LSN.063 June 1982.

[7] N.Tokuda and S.Yamada."New Formulation of the RFQ Radial Matching Section". Proc. 1981 Linear Accelerator Conf., October 19 – 23, 1981, Santa Fe, New Mexico, Los Alamos National Laboratory report LA – 9234 – C, (Feb. 1982),page 313.

[8] I.M.Kapchinskii and N.V.Lazarev."The Linear Accelerator Structure with Space – uniform Quadrupole Focusing" – IEEE Transactions on Nuclear Science, **NS – 26**, No.3, June 1979.

[9] T.P.Wangler."Space Charge Limits in Linear Accelerators" – LANL Internal Report. 1981.

[10] R.L.Gluckstern."Space Charge Effects" – Linear Accelerator. Ed.Lapostolle/Septier. p.827/836 (1970)

[11] W.D. Kilpatric. "Criterion for Vacuum Sparking Designed to Include Both rf and dc", Rev. Sci. Instrum. N.28, 824 (1957).

[12] IMS, RFQUICK, PARMTEQ and OUTTEST were written at LANL and kindly lent to CERN by K.Crandall.

[13] M.Weiss. "Bunching of Intense proton Beams with Six-dimensional Matching to the LINAC Acceptance". Proc. of the 1973 Particle Accelerator Conference, San Francisco, 5-7 March 1973.

[14] A.Lombardi,C.Biscari, and V.G.Vaccaro. "Surface Electric Field in an RFQ Linac". CERN Internal Report. in preparation.

APPENDIX A

MULTIPOLES COEFFICIENTS OF THE POTENTIAL FUNCTION IN THE RFQ.

An analytical computation of the multipole coefficients of the potential function is only an indication on the effects that the finite shape of the electrodes causes on the beam dynamics, if the series of Eq.(1.3.6) is cut at a given term. An exact computation would require a system of infinite equations, where the dimensions and characteristics of the tank which contains the vanes were also included.

The values of A_{ij} are obtained from boundary conditions imposed to the potential function and to the geometry of the electrodes.

We have begun from a simple case: we cut the series at the duodecapolar term (as in Eq.(4.2.1)) and we impose the following three conditions on the potential:

i. $U(a,0,0) = V/2$

ii. $U(ma,0,\beta\lambda/2) = V/2$

iii. $U(r_0,0,\beta\lambda/2) = V/2$

and the fourth condition is on the value of the transverse radius of curvature at the vane tip in the middle of the cell:

iv. $\rho(r_0,0,\beta\lambda/4) = \rho_0 = r^2U_r/(rU_r + U_{\theta\theta}) = \alpha r_0$

Sparing the time and patience of the reader, we give directly the solution of the system defined by these four equations:

$$A_{01} = 3(1+5\alpha)/[2r_0^2(1+7\alpha)] \qquad (A.1)$$

$$A_{03} = -(1+\alpha)/[2r_0^6(1+7\alpha)] \qquad (A.2)$$

$$A_{10} = [X\, I_4(mka) - Y\, I_4(ka)]/D \qquad (A.3)$$

$$A_{12} = [Y\, I_0(ka) - X\, I_0(mka)]/D \qquad (A.4)$$

with

$$D = I_0(ka)\, I_4(mka) - I_0(mka)\, I_4(ka) \qquad (A.5)$$

$$X = 1 - A_{01}A^2 - A_{03}A^6 \qquad (A.6)$$

$$Y = -(1 - A_{01}M^2A^2 - A_{03}M^6A^6) \qquad (A.7)$$

Observingthe shape of the vanes defined by the above coefficients (Figure 16), we see that they agree reasonably well with real vanes which are circular around the tip.

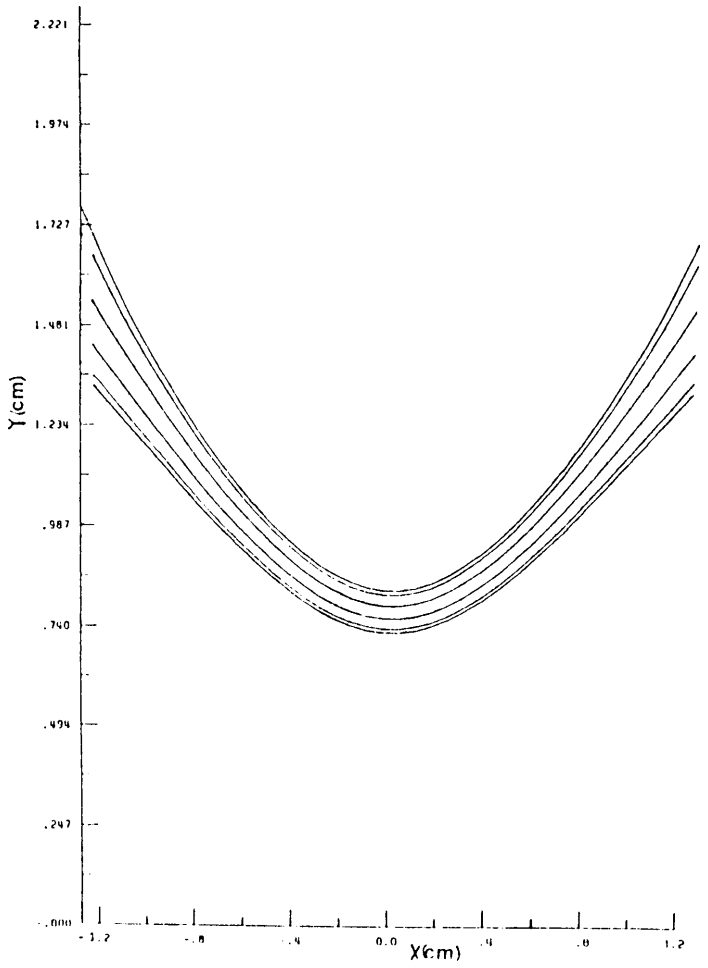

Figure 16: Transverse sections of the vane in the 12−polar approximation

To improve the approximation, we can add the 20−polar term ($A_{05}r^{10}\cos 10\theta$), and use a fifth condition:

v. $\rho(a,0,0) = \rho_0$

The results are illustrated in Figure 17

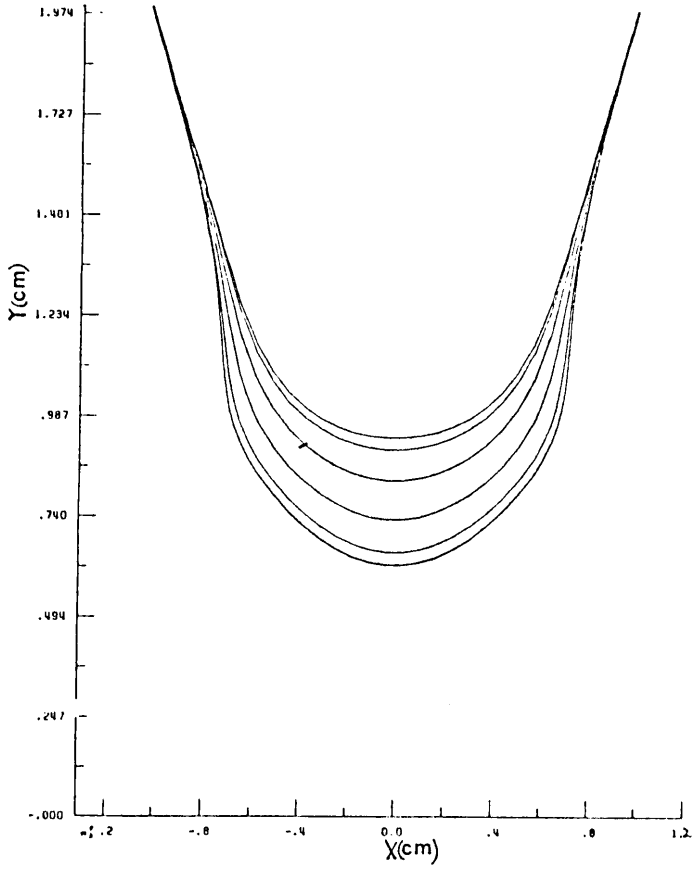

Figure 17: Transverse sections of the vane in the 20−polar approximation

APPENDIX B

COEFFICIENTS OF THE POTENTIAL FUNCTION IN THE RMS

The potential function in the RMS is (see Eq.(2.1.10)):

$$U(r,\theta,z) = V/2\,[\,A_q\, q(r,z)\cos 2\theta + A_d\, d(r,z)\cos 6\theta\,] \tag{B.1}$$

q(r,z) and d(r,z) are given in Eqs.(2.1.11). We define

$$\begin{aligned} q_0 &= q(r_0, L_{RMS}) \\ d_0 &= d(r_0, L_{RMS}) \end{aligned} \tag{B.2}$$

From the boundary condition

$$U(r_0, 0, L_{RMS}) = V/2 \tag{B.3}$$

we obtain the relationship between the coefficients A_q and A_d:

$$A_d = (1 - A_q q_0) / d_0 \tag{B.4}$$

The transverse section of the equipotential surface at a given $z = z_0$ is represented by the equation

$$S(r,\theta) = A_q q(r,z_0)\cos 2\theta + A_d d(r,z_0)\cos 6\theta \tag{B.5}$$

The transverse radius of curvature is:

$$\rho = [r^2 + (dr/d\theta)^2]^{3/2} / [r^2 + 2(dr/d\theta)^2 - r d^2r/d\theta^2] \tag{B.6}$$

At the vane tip ($\theta = 0$, $dr/d\theta = 0$) it can be then written as

$$\rho = r^2 / (r - d^2r/d\theta^2) \tag{B.7}$$

Differentiating Eq.(B.5) twice with respect to θ, we obtain:

$$d^2r/d\theta^2 = (2S_{r\theta}S_\theta S_r - S_{\theta\theta}S_r^{\,2} - S_{rr}S_\theta^{\,2}) / S_r^{\,3} \tag{B.8}$$

where the subscripts x_i stay for $\partial/\partial x_i$

Substituting in (B.7) and rearranging the terms we have:

$$\rho = r^2 S_r / (rS_r + S_{\theta\theta}) \tag{B.9}$$

We impose now the condition on ρ at $z = L_{RMS}$:

$$\rho(r_0, 0, L_{RMS}) = \rho_0 = \alpha r_0$$

and we obtain the value of A_q:

$$A_q = \frac{36\alpha d_0 - r_0 d_{0_r}(\alpha - 1)}{(\alpha - 1)r_0(q_{0_r} d_0 - q_0 d_{0_r}) + 32\alpha q_0 d_0} \tag{B.10}$$

where

$$q_{0_r} = \partial q/\partial r|_{r=r_0, z=L_{RMS}} \tag{B.11}$$

and analogously d_{0_r} . If ρ_0 is equal to the distance between the axis and the vane, r_0, at $z = L_{RMS}$, A_q and A_d are:

$$\begin{aligned} A_q &= 9/(8q_0) \\ A_d &= -1/(8d_0) \end{aligned} \tag{B.12}$$